Nuclear Science and Engineering

ISSN: (Print) (Online) Journal homepage: https://www.tandfonline.com/loi/unse20

Prediction of the Power Peaking Factor in a Boron-Free Small Modular Reactor Based on a Support Vector Regression Model and Control Rod Bank Positions

Priscila Palma Sanchez & Adimir dos Santos

To cite this article: Priscila Palma Sanchez & Adimir dos Santos (2021) Prediction of the Power Peaking Factor in a Boron-Free Small Modular Reactor Based on a Support Vector Regression Model and Control Rod Bank Positions, Nuclear Science and Engineering, 195:5, 555-562, DOI: 10.1080/00295639.2020.1854541

To link to this article: https://doi.org/10.1080/00295639.2020.1854541

NUCLEAR SCIENCE AND ENGINEERING · VOLUME 195 · 555–562 · MAY 2021

DOI: https://doi.org/10.1080/00295639.2020.1854541

Check for updates

ANS

Technical Note

Prediction of the Power Peaking Factor in a Boron-Free Small Modular Reactor Based on a Support Vector Regression Model and Control Rod Bank Positions

Priscila Palma Sanchez* and Adimir dos Santos
Instituto de Pesquisas Energéticas e Nucleares, IPEN–CNEN/SP, Brazil

Received June 1, 2020
Accepted for Publication November 17, 2020

Abstract — *In order to ensure safety in a nuclear power plant, operation and protection systems must take into account safety parameters, whether to guide operators or to trip the reactor in emergency cases. Especially in a boron-free small modular reactor (SMR) where reactivity and power are controlled exclusively by rod banks, the power distribution is mostly influenced by its movements affecting the power peaking factor (PPF), which is an important parameter to be considered. The PPF relates the maximum local linear power density to the average power density in a fuel rod indicating a high neutron flux that can cause fuel rod damage. In this technical note, 2117 samples from simulations of an idealized boron-free SMR controlled exclusively by rod banks were used to generate a Support Vector Machine (SVM) model capable of estimating the PPF as a function of control rod bank positions. Such model could be used to predict the maximum PPF in the reactor core by carrying out simple calculation. Residing in a SVM parameter grid search and a 10-cross-validation process in the training set to reach an optimized and robust model, the results have shown a root-mean-squared error of about 0.1% consistent for both training and testing sets.*

Keywords — *Support vector, power peaking factor, small modular reactor, reactor monitoring, boron free.*

Note — *Some figures may be in color only in the electronic version.*

I. INTRODUCTION

Growth in Artificial Intelligence (AI) has made it possible to approach problems through machine learning techniques; consequently, a substantial quantity of work has been produced in the last few years in distinct areas of expertise.[1–5] However, even with all the computational capability available nowadays and modern approaches being sought in the nuclear field, it would not be practical to calculate every reactor state from physics-based simulations during plant operation and use it in monitoring and controlling systems because in addition to the reactor calculation itself, postprocessing would be highly time-consuming considering the timescale response desired for such systems. Thus, reactor technology endeavors to use AI techniques for simpler and accurate models that could be applied in control and diagnosis to predict parameters generally associated with reactor safety such as critical heat flux and power peaking factor (PPF), among others.[6–13]

As one of these parameters of interest, the PPF is of great importance and shall be fully monitored during operation, especially in boron-free small modular reactors (SMRs) in which reactivity control and power are exclusively performed by rod banks. For some current SMR designs that rely on such characteristics [the CAREM reactor from CNEA and IMR from Mitsubishi, for example],[14] the required monitoring conditions could present a challenge for safe operation. In these reactors, control rod banks must be more inserted in the core during operation when compared with a standard Pressurized Water Reactor (PWR), in which a significant part of the reactivity is controlled by boric acid diluted in the moderator; consequently, the nonhomogeneous control rod absorber presence causes a major neutron flux distortion affecting power distribution and fuel rod temperature profile.

*E-mail: priscila.sanchez@usp.br

As the PPF relates the maximum local linear power density (LPD) to the average power density in a fuel rod, it can indicate the level of neutron flux distortions inside the reactor core.

In SMRs, PPF online monitoring could be performed using in-core detectors such as Self-Powered Neutron Detectors (SPNDs) and operational ex-core detectors. However, some issues must be addressed in order to obtain more suitable and reliable systems for SMR designs and their operational conditions, especially those for propulsion purposes, which operate as load-follower requiring automatic control rod bank movements. First, the prompt-signal cobalt SPNDs available in the nuclear industry are much less accurate than rhodium detectors, which have a slower response time,[15] and a delay would also be added in the process of calculating the PPF from the in-core power distribution map. Second, SMR proportions are comparable to the ex-core detector's sensitive dimensions, which could cause unrealistic power distribution measurements along the axial direction, as the ex-core detectors placed in the upper and lower parts of the reactor vessel surroundings could not effectively discriminate the contribution of each active core portion in the overlay signal. Consequently, considering these existing limitations and constraints, an approach that uses AI techniques could be exploited in the new SMR developments.

In the last few decades, there has been special interest in SMRs [under 300 MW(electric)] for generating electricity from nuclear power, pursuing passive safety systems, reducing capital costs, and providing power to regions far off the grid distribution systems.[14] A remarkable feature of these small new designs is the possibility of modular construction, where large mechanical and structural reactor parts can be mounted off-site and then brought into place. Moreover, these small, simpler units are also strategic in the case of ship and submarine compact vessels with greater propulsion availability for military use as well as for merchant objectives.[16,17] Currently, SMRs based on diverse concepts are under development or construction. Most of them are in the conceptual phase, and some are licensed (SMART, Korea), under construction (HTR-PM China; KLT-40S Russia; CAREM, Argentina), or already in operation (IPHWR-220, India).[18]

As an approach for reactor plant control and safety monitoring during operation, some researchers have used AI techniques to estimate the PPF. Most of them have used Artificial Neural Networks[19–22] (ANNs), and a few have used Support Vector Machine[23,24] (SVM). However, none of them have addressed the behavior of such tools in boron-free SMRs. The previous published works in which PPF estimation is approached through the SVM tool[23,24] employed it in a standard commercial reactor. The standard reactor has a much longer active size, and the PPF will differ in behavior when compared with a boron-free SMR, mainly because of the nonhomogeneous xenon distribution and relatively less insertion of control rods in the core. Therefore, the feasibility of SVM modeling and its characteristics have not yet been exploited in boron-free SMRs. Regarding the methods, the selection of train and test datasets and model validation during training in addition to the dataset size and model complexity may also vary from this technical note to similar studies covering the subject.

The AI technique called SVM is based on machine learning and it was first applied in classification problems, but lately, it has also been used to solve nonlinear regression problems by minimizing an alternative loss function.[25] Its mechanism involves mapping the problem into a space in which it becomes linear and simple to solve. Consequently, using the alternative loss function, SVM can be applied to accurately estimate the PPF (Refs. 23 and 24) presenting some advantages over the ANN method[23,26] such as greater sensitivity in dealing with monotonic transformations and values containing irrelevant input information, better generalization performance and interpretability of the logic behind the algorithm, etc.

The work presented in this technical note was performed using an idealized small modular boron-free PWR in order to create a SVM model and evaluate its accuracy in predicting the PPF in reactors with such peculiar characteristics. For this purpose, the reactor simulations were carried out in the three-dimensional (3-D) multigroup diffusion code CITATION[27] aiming to obtain the PPF for distinct configurations of control rod bank positions and use it as input in the process of building an adequate SVM model in R code.[28] The diffusion code was merely applied to obtain the database to investigate the SVM concept in these sorts of reactors; therefore, a higher-order code based on neutron transport methods could also be employed in the reactor modeling without becoming restrictive.

II. METHODOLOGY

II.A. Support Vector Machine

Support Vector Machine (SVM) is a statistical tool based on machine learning that was first introduced by Vapnik and Chervonenkis in the 1960s (Ref. 29). It is commonly used in classification problems and pattern recognition, but it is also possible to solve regression problems by introducing an alternative loss function known as ε-insensitive.

The main idea of Support Vector Regression (SVR) is mapping a nonlinear problem into a high-dimensional feature space where it becomes linear and easier to solve. Therefore, given a set of N training data $\{(\boldsymbol{x}_i, y_i)\}_{i=1}^{N} \in \Re^n \times \Re$, with $\boldsymbol{x}_i$ being the state input vector and y_i being the desired value to be predicted by the SVR model, the following regression function can be considered:

$$y = f(\boldsymbol{x_i}, \boldsymbol{w}) = \sum_{j=1}^{n} \omega_j \phi_j(\boldsymbol{x_i}) + b = \langle \boldsymbol{w},\ \boldsymbol{\Phi}(\boldsymbol{x_i}) \rangle + b$$

with

$$\boldsymbol{w} = [\omega_1 \omega_2 \ldots \omega_n]$$

and

$$\boldsymbol{\Phi} = [\phi_1 \phi_2 \ldots \phi_n] \ ,$$

where

$\boldsymbol{\Phi}$ = feature that maps $\boldsymbol{x}_i$ vectors in the n-dimensional space

$\boldsymbol{w}$ = weight vectors

b = bias.

The optimization problem consists of minimizing the regularized risk function:

$$R(\boldsymbol{w}) = \frac{1}{2} \| \boldsymbol{w} \|^2 + C \sum_{i=1}^{N} |y_i - f(\boldsymbol{x}_i, \boldsymbol{w})|_\varepsilon \ , \tag{1}$$

where

$$|y_i - f(\boldsymbol{x}_i, \boldsymbol{w})|_\varepsilon = \begin{cases} 0, & \text{if } |y_i - f(\boldsymbol{x}_i, \boldsymbol{w})| \leqslant \varepsilon \\ |y_i - f(\boldsymbol{x}_i, \boldsymbol{w})| - \varepsilon, & \text{otherwise.} \end{cases}$$

The term $|y_i - f(\boldsymbol{x}_i, \boldsymbol{w})|_\varepsilon$ is the so-called Vapnik's ε-insensitive loss function that defines a tube around $f(\boldsymbol{x}_i, \boldsymbol{w})$. If y_i lies inside the tube, then the ε-insensitive loss function is zero, and if it is located outside, the function gives the distance between y_i and the tube boundary. The parameter C is the regularization constant determining the trade-off between $f(\boldsymbol{x}_i, \boldsymbol{w})$ flatness and the amount up to which deviations larger than ε are tolerated in the regression function. Increasing ε causes a reduction in the number of support vectors as well as in the bias term; however, it decreases model accuracy leading to overfitting issues.

From Eq. (1), it is possible to notice that larger errors can be penalized by increasing either C or although as increasing the weight vector norm would cause model complexity to rise, the general course of action is to minimize the risk function by tuning the regularization constant and the loss function deviation threshold.

Equation (1) can be rewritten as a function of upper $\boldsymbol{\xi}^*$ and lower $\boldsymbol{\xi}$ constraints on the system's outputs as

$$R(\boldsymbol{w}, \xi, \xi^*) = \frac{1}{2} \| \boldsymbol{w} \|^2 + \boldsymbol{C} \sum_{i=1}^{N} \left(\boldsymbol{\xi_i} + \boldsymbol{\xi_i^*} \right) \ , \tag{2}$$

where

$$\boldsymbol{\xi} = [\xi_1 \xi_2 \ldots \xi_N]$$

and

$$\xi^* = \left[\xi_1^* \xi_2^* \ldots \xi_N^* \right]$$

with the following constraints:

$$\begin{cases} y_i - \langle \boldsymbol{w}, \boldsymbol{\Phi}(\boldsymbol{x}_i) \rangle - b \leqslant \varepsilon + \xi_i \\ \langle \boldsymbol{w}, \boldsymbol{\Phi}(\boldsymbol{x}_i) \rangle + b - y_i \leqslant \varepsilon + \xi_i^* \\ \xi_i, \xi_i^* \geqslant 0 \,. \end{cases} \quad \text{for } i = 1, 2, 3, \ldots, N \tag{3}$$

Then, the Lagrangian composed by Eq. (2) and the constraints in Eq. (3) gives the final regression function

$$y = f(\boldsymbol{x}_k) = \sum_{i=1}^{N} (\alpha_i - \alpha_i^*) K(\boldsymbol{x}_i, \boldsymbol{x}_k) + b \ , \tag{4}$$

where $K(\boldsymbol{x}_i, \boldsymbol{x}_k) = \langle \boldsymbol{\Phi}(\boldsymbol{x}_i), \boldsymbol{\Phi}(\boldsymbol{x}_k) \rangle$ is the kernel function. If y_i lies outside the ε-tube, then either the α_i or the α_i^* Lagrange coefficient is nonzero, and the corresponding observation $\boldsymbol{x}_i$ is called a support vector. Thereby, from Eq. (4), any other predicted value y could be obtained from its associated observations or state input vector $(\boldsymbol{x}_k)$ just as a function of the support vectors.

Figure 1 shows a scheme for better visualization of a nonlinear SVR using Vapnik's ε-insensitive loss function, including its constraints.

This technical note uses the Radial Basis Function (RBF) or Gaussian kernel given by

$$K(\boldsymbol{x}_i, \boldsymbol{x}_k) = e^{-\gamma \|\boldsymbol{x}_i - \boldsymbol{x}_k\|^2} \ .$$

The RBF maps the real-world data into the feature space where a linear model can be built and easily solved.

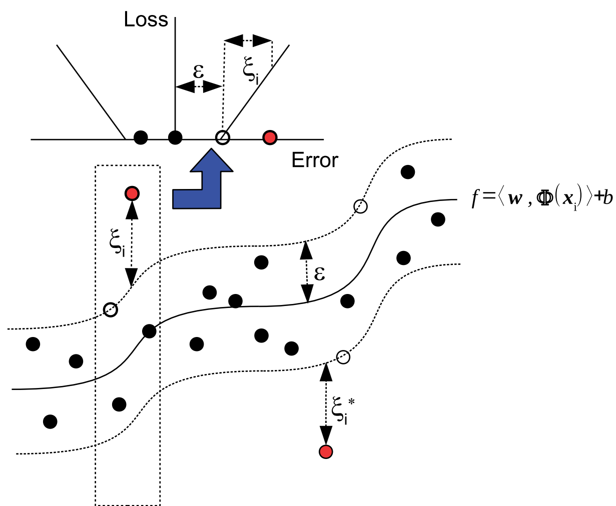

Fig. 1. Nonlinear SVR scheme with Vapnik's ε-insensitive loss function. Adapted from Ref. 30.

The SVM tool is very sensitive to the choice of proper parameters.[31] So, in order to apply the demonstrated method above, it is recommended to use a grid search over all hyperparameters available (C, ε, γ) to reach better results. The grid search can be employed simply by selecting a finite set of reasonable values for each hyperparameter, training the data with each combination of these sets, evaluating performance by internal k-fold cross-validation, and keeping the parameters that achieved the highest score in the validation process. This validation method gives a trade-off between model bias and variance: the lower the k-value, the higher is the bias in the error estimate and the smaller is the variance. Conversely, when the k-value is set equal to the number of instances in the training set, the error estimate is then very low in bias but has a high variance potential.

Genetic algorithms and other tools can also be implemented to find the best model parameter values, although they are computationally highly demanding and for small datasets most of the time present very similar results when compared with simple methods such as grid search, for example.[31–33]

The approach adopted in this technical note to create the SVM model is a grid search using exponents of 2 for C and γ along with a 10-cross-validation process in the training set, which is recommended for well-balanced bias and variance.[34] Subsequently, the C and γ ranges were reduced around each better result from the previous search aiming to fine-tune the values, and then, after finding the best values for these two hyperparameters, a similar procedure was applied for the ε loss function parameter keeping the other two fixed.

II.B. Reactor Model Description and PPF Estimation

The simulated SMR selected to acquire the SVM input database was modeled in the 3-D multigroup code CITATION[27] designed by Oak Ridge National Laboratory to solve problems using the finite difference representation of the neutron diffusion theory as a simplification of the neutron transport equation. In order to idealize the reactor, a typical standard western PWR design was chosen: 275°C average moderator temperature, 135-bar primary circuit pressure, one fuel cycle, uniform slightly enriched UO_2 pellets surrounded by Zircaloy cladding, 17 × 17 rectangular assembly array possessing 29 guide tubes for control or safety rods comprising 21 fuel assemblies in the full core. The active length considered was approximately one meter long.

Initially, the focus of the reactor core configuration with safety and control banks was on covering a sufficient reactor shutdown margin in the cold and stuck rod condition as well as the existing reactivity excess without boron diluted in the moderator. The model considered three control rod banks (C1, C2, and C3), uniformly distributed in the reactor core in order to ensure a more balanced power distribution during the first cycle of operation, and two safety banks (S1 and S2) located at the periphery of the reactor. Furthermore, burnable poison rods (about 20) were inserted and equally distributed inside the fuel assembly located in the reactor middle with the purpose of flattening the power distribution curve on the region.

The simulations were performed in four energy groups, with bank C3 fully inserted, banks S1 and S2 completely withdrawn, while banks C1 and C2 could vary from withdrawn to fully inserted aiming to cover as many as possible operational situations during fuel burning. These are representative scenarios as the changes occurring in the core along the cycle are mainly related to the introduction of neutron-absorbing fission products that would just cause the reactor to operate with control rod banks more withdrawn.

The PPF was calculated from simulations as

$$\mathrm{PPF} = \frac{\max\{\mathrm{LPD}\}}{P_t/(M \cdot l)}$$

with

$$\mathrm{LPD} = \kappa \cdot A_t \cdot \sum_{g=1}^{4} \sigma_{f,g} \cdot \phi_g \ ,$$

where

P_t = total thermal power
M = total number of fuel rods
l = active length
κ = average energy released per fission
$\sigma_{f,g}$ = macroscopic fission cross section per energy group g
A_t = transversal area of the mesh size region
ϕ_g = neutron flux crossing the mesh region.

III. RESULTS

The database acquired using the CITATION simulations from 2117 possible configurations of the C1 and C2 control rod banks has shown a peaking factor range varying from approximately 2 to 3.2. As can be seen in Figs. 2 and 3, the PPF behavior is represented by a smooth surface, and the region where the PPF is above 3 can be observed when both banks are around 50 to 70 cm inserted in the core (more than half the total core active length).

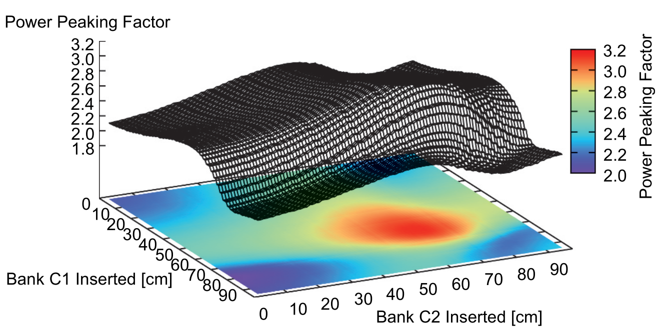

Fig. 2. Three-dimensional and two-dimensional PPF behavior according to bank C1 and bank C2 insertion in the reactor core.

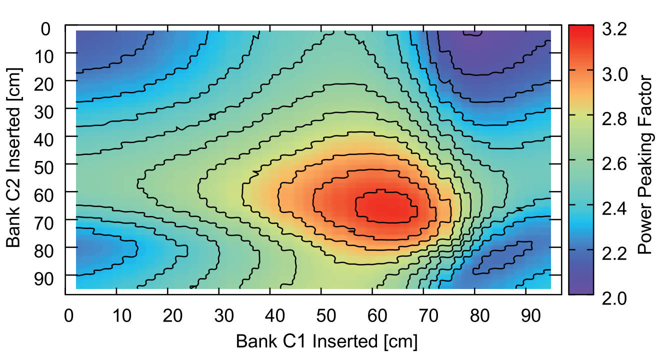

Fig. 3. Two-dimensional detail and level curves of PPF behavior according to bank C1 and bank C2 insertion in the reactor core.

Figure 3 also shows that the PPF is the highest when the C1 and C2 banks are positioned approximately 66 cm inside the core (around two-thirds of it). The presented behavior can be easily explained since in a thermal reactor neutronically loosely coupled, the axial neutron flux shows a half-cosine shape that is pushed toward the bottom of the core by the insertion of the control rod banks.

The step positions of banks C1 and C2 were used as input and the PPF as the output in the SVR model obtained from R code.[28] Initially, the data were randomly split into training set $\left\{\left(x_i^{C1}, x_i^{C2}, y_i^{PPF}\right)\right\}_{i=1}^{1589}$ (75%) and testing set $\left\{\left(x_k^{C1}, x_k^{C2}, y_k^{PPF}\right)\right\}_{k=1}^{528}$ (25%), and then, the parameter grid searches were performed over the training set by means of the tune function intending to create the model.

A large grid search was completed using exponents of 2 for both C and γ over the training set, followed by subsequent searches reducing the exponent range and grid size around the best values found as previous results. A total of four searches of this kind was executed. Then, the final values of these two hyperparameters were found by using a smaller range and a more refined grid around them. After selecting the final values of C and γ and fixing them, two ε grid searches were performed around small values aiming to improve the model accuracy accordingly with the loss function properties. The final model was also built using the tune function default 10-cross-validation procedure, as recommended for well-balanced bias and variance.[34] The best model performance was reached with $C = 256$, $\gamma = 2$, and $\varepsilon = 0.01$ and 482 support vectors.

The testing set presented a very similar performance to that obtained in the training set, as shown in Table I, proving the model generalization power in estimating the PPF for a variety of reactor conditions. Statistical errors were very low, highlighted by the Root-Mean-Squared Error (RMSE) of about 0.1%. Although, the maximum relative error could be considered quite high, around 1%, the frequency distribution in Fig. 4 is mostly concentrated in the ±0.2% range.

The Willmott's Index of Agreement is a standardized measure of the degree of model prediction error, ranging

TABLE I

Training and testing set statistical error analysis.

Dataset	RMSE (%)	Maximum Relative Error (%)	Mean Absolute Error, 10^{-3}	Willmott's Index of Agreement
Training	0.15	1.45	2.3	0.9999994
Testing	0.16	1.05	2.6	0.9999993

 ANS

from zero to one. The value of one indicates a perfect match between predicted and observed data while zero indicates no agreement at all.[35] That being said, the index presented in Table I corroborates with the high model accuracy seen in Figs. 5 and 6 where most of the predicted PPF values overlap the simulated ones for both training and testing sets.

Finally, Fig. 7 also indicates that PPF residues obtained from the prediction model when compared with the CITATION simulations results weighted by its standard deviations show a Gaussian characteristic expected from a reliable regression model: points are symmetrically distributed around zero with approximately 65% of them between ±1, 95% between ±2, and 99% between ±3.

Supposing the PPF value of the idealized reactor considered is limited by design in less than 3, this would lead to restrictions in some bank position combinations with the purpose of preventing core damage and ensure safety. In order to fulfill this requirement, the maximum operation reactor power or the automation system complexity could be affected depending on the uncertainty of the PPF monitoring technique employed. However, as the SVM approach showed a high level of accuracy in predicting the PPF, there would be no further complications related to it, demonstrating its possible applicability on monitoring PPF in boron-free SMR with all the advantages previously highlighted.

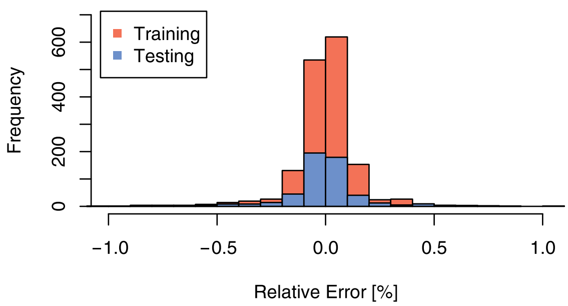

Fig. 4. Training and testing set relative error distribution.

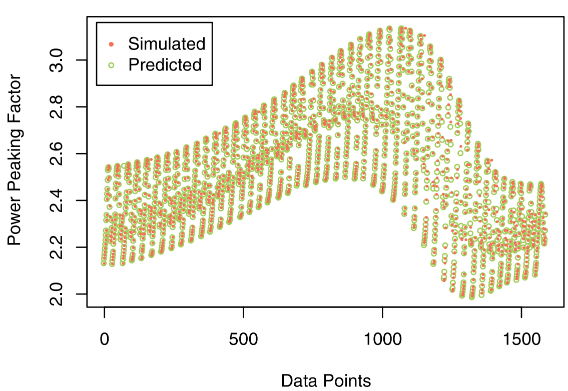

Fig. 5. CITATION-simulated and SVM-predicted PPF from the training set.

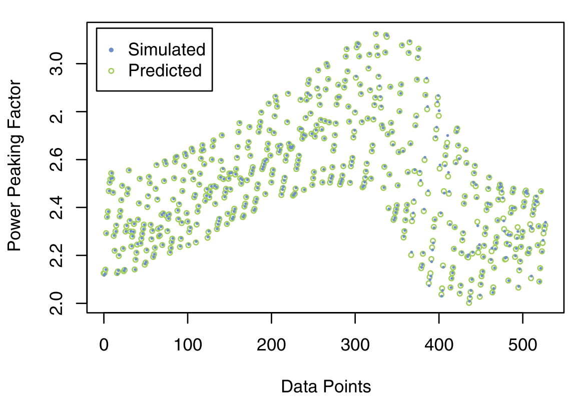

Fig. 6. CITATION-simulated and SVM-predicted PPF from the testing set.

IV. CONCLUSIONS

The SVR has presented itself as a promising approach to estimate the PPF with a high level of confidence and generalization without calculating every reactor state from physics-based simulations during operation of boron-free SMRs controlled exclusively by rod banks movement. The relatively small number of support vectors (model simplicity) turns calculations fast and viable to be employed in online PPF prediction, overcoming the above-mentioned issues of the monitoring systems commonly used in PWRs.

It is possible that statistical errors could be reduced even more by adding new reactor inputs to the SVR model as, for example, the neutron thermal flux in the in-core nuclear detector positions. Meanwhile, it has not showed significant performance improvements in the testing set for general commercial PWRs (Ref. 23). Another change that could be implemented in the SVR model is the database increase with nonsymmetrical rod position configurations (decoupling each control rod from the rod banks) intending

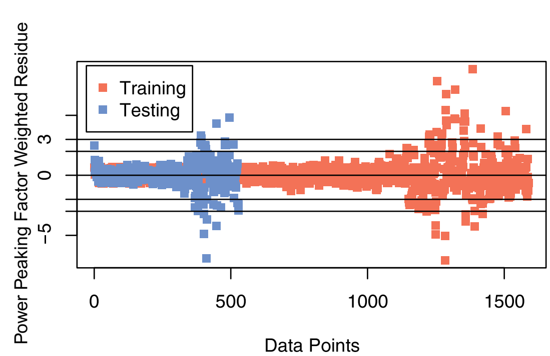

Fig. 7. Training and testing set PPF weighted residue.

to build a model capable of predicting, with greater reliability, more general reactor configurations including those faced in accident conditions and thereby giving more flexibility to manage the PPF in case of anomalies.

Acknowledgments

The authors would like to thank Alfredo Abe, Pamela Piovezan, Thiago Carluccio, Gregório Souza, and Delvonei Andrade as well as Natália Carvalho for all guidance. This research did not receive any specific grant from funding agencies in the public, commercial, or not-for-profit sectors.

ORCID

Priscila Palma Sanchez http://orcid.org/0000-0002-4592-7534
Adimir dos Santos http://orcid.org/0000-0002-5989-5705

References

1. M. R. PHANGTRIASTU, J. HAREFA, and D. F. TANOTO, "Comparison Between Neural Network and Support Vector Machine in Optical Character Recognition," *Procedia Comput. Sci.*, **116**, 351 (2017); https://doi.org/10.1016/j.procs.2017.10.061.

2. W. WU et al., "A Comparison of Support Vector Machines, Artificial Neural Network and Classification Tree for Identifying Soil Texture Classes in Southwest China," *Comput. Electron. Agric.*, **144**, 86 (2018); https://doi.org/10.1016/j.compag.2017.11.037.

3. N. A. BHASKAR, "Performance Analysis of Support Vector Machine and Neural Networks in Detection of Myocardial Infarction," *Procedia Comput. Sci.*, **46**, 20 (2015); https://doi.org/10.1016/j.procs.2015.01.043.

4. H. LI and F. SUN, "Comparative Studies of Alignment, Alignment-Free and SVM Based Approaches for Predicting the Hosts of Viruses Based on Viral Sequences," *Sci. Rep.*, **8**, 10032 (2018); https://doi.org/10.1038/s41598-018-28308-x.

5. S. M. GIZAW and T. Y. GAN, "Regional Flood Frequency Analysis Using Support Vector Regression Under Historical and Future Climate," *J. Hydrol.*, **538**, 387 (2016); https://doi.org/10.1016/j.jhydrol.2016.04.041.

6. B. T. JIANG and F. Y. ZHAO, "Combination of Support Vector Regression and Artificial Neural Networks for Prediction of Critical Heat Flux," *Int. J. Heat Mass Transfer*, **62**, 481 (2013); https://doi.org/10.1016/j.ijheatmasstransfer.2013.03.025.

7. J. CAI, "Applying Support Vector Machine to Predict the Critical Heat Flux in Concentric-Tube Open Thermosiphon," *Ann. Nucl. Energy*, **43**, 114 (2012); https://doi.org/10.1016/j.anucene.2011.12.029.

8. B. T. JIANG et al., "Prediction of Critical Heat Flux for Water Flow in Vertical Round Tubes Using Support Vector Regression Model," *Prog. Nucl. Energy*, **68**, 210 (2013); https://doi.org/10.1016/j.pnucene.2013.07.004.

9. J. LIU et al., "Nuclear Power Plant Components Condition Monitoring by Probabilistic Support Vector Machine," *Ann. Nucl. Energy*, **56**, 23 (2013); https://doi.org/10.1016/j.anucene.2013.01.005.

10. S. G. KIM, Y. G. NO, and P. H. SEONG, "Prediction of Severe Accident Occurrence Time Using Support Vector Machines," *Nucl. Eng. Technol.*, **47**, 74 (2015); https://doi.org/10.1016/j.net.2014.10.001.

11. K. H. YOO et al., "Prediction of Golden Time Using SVR for Recovering SIS Under Severe Accidents," *Ann. Nucl. Energy*, **94**, 102 (2016); https://doi.org/10.1016/j.anucene.2016.02.029.

12. X. JUNCAI, R. QINGWEN, and S. ZHENZHONG, "Prediction of the Strength of Concrete Radiation Shielding Based on LS-SVM," *Ann. Nucl. Energy*, **85**, 296 (2015); https://doi.org/10.1016/j.anucene.2015.05.030.

13. Y. ZENG et al., "Machine Learning Based System Performance Prediction Model for Reactor Control," *Ann. Nucl. Energy*, **113**, 270 (2018); https://doi.org/10.1016/j.anucene.2017.11.014.

14. "Advances in Small Modular Reactor Technology Developments: A Supplement to IAEA Advanced Reactors Information System (ARIS), 2018," International Atomic Energy Agency; https://aris.iaea.org/Publications/SMR-Book_2018.pdf (current as of Apr. 20, 2020).

15. W. H. TODT, "Characteristics of Self-Powered Neutron Detectors Used in Power Reactors," *Proc. Specialists' Mtg. In-Core Instrumentation and Core Assessments*, Mito-Spi, Japan, October 14–16, 1996, p. 181, Organisation for Economic Co-operation and Development, Nuclear Energy Agency (1997); https://www.oecd-nea.org/science/rsd/ic96/4-2.pdf (current as of Apr. 20, 2020).

16. A. R. NEWHOUSE, "Ship Nuclear Propulsion," McGraw-Hill (2014); https://www.accessscience.com/content/ship-nuclear-propulsion/619700 (current as of Jan. 7, 2020).

17. L. O. FREIRE and D. A. DE ANDRADE, "Historic Survey on Nuclear Merchant Ships," *Nucl. Eng. Des.*, **293**, 176 (2015); https://doi.org/10.1016/j.nucengdes.2015.07.031.

18. Advanced Reactors Information System (ARIS) website; https://aris.iaea.org/sites/SMR.html, International Atomic Energy Agency (current as of Jan. 7, 2020).

19. M. G. NA et al., "Estimation of the Nuclear Power Peaking Factor Using In-Core Sensor Signals," *J. Korean Nucl. Soc.*, **36**, 420 (2004).

20. J. L. MONTES et al., “Local Power Peaking Factor Estimation in Nuclear Fuel by Artificial Neural Networks,” *Ann. Nucl. Energy*, **36**, 121 (2009); https://doi.org/10.1016/j.anucene.2008.09.011.
21. A. PIROUZMAND and M. K. DEHDASHTI, “Estimation of Relative Power Distribution and Power Peaking Factor in a VVER-1000 Reactor Core Using Artificial Neural Networks,” *Prog. Nucl. Energy*, **85**, 17 (2015); https://doi.org/10.1016/j.pnucene.2015.06.001.
22. J. H. BACK et al., “Prediction and Uncertainty Analysis of Power Peaking Factor by Cascaded Fuzzy Neural Networks,” *Ann. Nucl. Energy*, **110**, 989 (2017); https://doi.org/10.1016/j.anucene.2017.08.006.
23. I. H. BAE et al., “Calculation of the Power Peaking Factor in a Nuclear Reactor Using Support Vector Regression Models,” *Ann. Nucl. Energy*, **35**, 2200 (2008); https://doi.org/10.1016/j.anucene.2008.09.004.
24. I. H. BAE et al., “Estimation of the Power Peaking Factor in a Nuclear Reactor Using Support Vector Machines and Uncertainty Analysis,” *Nucl. Eng. Technol.*, **41**, 1181 (2009); https://doi.org/10.5516/NET.2009.41.9.1181.
25. A. J. SMOLA, B. SCHÖLKOPF, and K. R. MÜLLER, “General Cost Functions for Support Vector Regression,” *Proc. 9th Australian Conf. Neural Networks*, Brisbane, Queensland, Australia, 1998, p. 79 (1998).
26. M. G. FERNANDEZ et al., “Status of Research and Development of Learning-Based Approaches in Nuclear Science and Engineering: A Review,” *Nucl. Eng. Des.*, **359**, 110479 (2020); https://doi.org/10.1016/j.nucengdes.2019.110479.
27. T. B. FOWLER, D. R. VONDY, and G. W. CUNNINGHAM, “Nuclear Reactor Core Analysis Code: CITATION,” ORNL-TM-2496, Rev. 2, Oak Ridge National Laboratory (1971).
28. R CORE TEAM, “R: A Language and Environment for Statistical Computing,” R Foundation for Statistical Computing (2013); http://www.R-project.org/ (current as of June 1, 2020).
29. V. VAPNIK, *Statistical Learning Theory*, John Wiley & Sons, New York (1998).
30. S. RAGHAVENDRA and P. DEKA, “Support Vector Machine Applications in the Field of Hydrology: A Review,” *Appl. Soft Comput.*, **19**, 372 (2014); https://doi.org/10.1016/j.asoc.2014.02.002.
31. D. MEYER, “Support Vector Machines. The Interface to Libsvm in Package E1071,” Online-documentation of the package e1071 for R, Technische Universität Wien (2001).
32. S. YUANYUAN et al., “The Comparison of Optimizing SVM by GA and Grid Search,” *Proc. IEEE 13th Int. Conf. Electronic Measurement and Instruments*, Yangzhou, China, October 20–22, 2017, p. 354, Institute of Electrical and Electronics Engineers (2017).
33. I. SYARIF, A. PRUGEL-BENNETT, and G. WILLS, “SVM Parameter Optimization Using Grid Search and Genetic Algorithm to Improve Classification Performance,” *TELKOMNIKA*, **14**, 1502 (2016); https://doi.org/10.12928/telkomnika.v14i4.3956.
34. M. KUHN and K. JOHNSON, *Applied Predictive Modelling*, Springer, New York (2018).
35. H. R. PEREIRA et al., “On the Performance of Three Indices of Agreement: An Easy-to-Use R-Code for Calculating the Willmott Indices,” *Bragantia*, **77**, 394 (2018); https://doi.org/10.1590/1678-4499.2017054.